JCTC Journal of Chemical Theory and Computation

Neutral and Anionic Gold Decamers: Planar Structure with Unusual Spatial Charge-Spin Separation

Young Cheol Choi,[†] Woo Youn Kim,[†] Han Myoung Lee,*[,‡] and Kwang S. Kim*[,†]

Center for Superfunctional Materials, Department of Chemistry, and Center for Basic Sciences, Pohang University of Science and Technology, San 31, Hyojadong, Namgu, Pohang 790-784, Korea

Received August 1, 2008

Abstract: We have investigated the issue of two-dimensional (2D) versus three-dimensional (3D) structures for neutral-state Au_{10} and clarified the lowest-energy structure among a few 2D Au_{10}^- isomers. Though almost all previous works were based on density functional theory (DFT), we here carried out not only extensive DFT calculations but also high levels of ab initio calculations of Möller-Plesset second order perturbation theory (MP2), and coupled cluster theory with single and double excitations (CCSD) including perturbative triple excitations [CCSD(T)]. While DFT favors 2D structures, MP2 and CCSD(T) favor 3D structures for moderate-sized basis sets. However, we note that the basis-set superposition error (BSSE) corrections make the ab intio results favor 2D structures too. The near-degeneracy (driven by relativistic effects) of 5d and 6s orbitals of gold helps stabilize acute apex gold atoms, resulting in 2D structures. The planar triangular structures of a local minimum Au_{10} (triplet) and the global minimum Au_{10}^- show remarkable spatial charge-spin separation due to their singly occupied molecular orbital(s). By the same reason, Au_{10}^- shows much larger vertical detachment energy than other even-numbered gold cluster anions.

I. Introduction

Nanoscale metal clusters[1] have received great attention as one of the most fundamental subjects of nanosize metallic materials[2] and devices.[3] These metal clusters can form an intriguing arrangement of atoms and often show unusual features for a certain specific size. Since gold is known to be a special novel metal showing effective s−d hybridization due to the large relativistic effect,[4] gold nanoclusters (Au_n) have been extensively investigated.[5,6] In particular, the lowest-energy structures of Au_{10} and Au_{10}^- are not clear. In particular, various two-dimensional (2D)[7−9] and three-dimensional (3D)[10] structures have been reported as possible global minimum energy structures for the neutral state, Au_{10}. In this regard, Au_{10} is likely to have the structures corresponding to the crossover region of the 2D to 3D transition. For the anion state, Au_{10}^-, Kappes, Ahlrichs, and co-workers[11] proved convincingly that Au_{10}^- is planar by comparing the experimentally measured ion mobility with DFT results. In addition, the presence of multiple isomers of planar Au_{10}^- is also known.[12] Landman and co-workers[8] have also reported 2D structures for Au_{10}^-. However, all these results were based on DFT calculations. Since DFT often tends to favor 2D structures over 3D structures,[7,13] a clear demonstration with ab initio methods such as Möller-Plesset second-order perturbation theory (MP2) and coupled cluster theory with single and double excitations including perturbative triple excitations [CCSD(T)] would be desirable.

In addition, the neutral and anionic gold decamers (Au_{10} and Au_{10}^-) show particularly unusual features such as large vertical-electron detachment energies (VDEs).[7−10,14,15] In general, odd-numbered gold cluster anions have large VDEs, and even-numbered gold cluster anions have small VDEs.[14,15] However, in the case of Au_{10}^-, an even-numbered cluster, the photoelectron spectrum (PES) shows a large VDE with

* Corresponding author e-mail: kim@postech.ac.kr (K.S.K.) or abcd0lhm@postech.ac.kr (H.M.L.).

[†] Center for Superfunctional Materials and Departments of Chemistry and Physics.

[‡] Department of Chemistry and Center for Basic Sciences.

10.1021/ct8003113 CCC: $40.75
Published on Web 04/24/2009

very small energy gap between the first and second main peaks.[14,15] Furthermore, we find unexpectedly large spatial charge−spin separation (SCSS) phenomena for Au_{10}^- and Au_{10}, which could be of importance for the study of spin dot devices. Here, we discuss these intriguing features, using DFT and high-level ab initio calculations.

II. Computational Details

We studied the system with DFT using two different functionals: (i) Becke's three-parameter exchange and Lee−Yang−Parr correlation functionals (B3LYP) was used with the Hay−Wadt valence double-ζ (VDZ) ($n + 1$) effective core potential (ECP) basis set (to be abbreviated as HW),[16] and (ii) the generalized gradient approximation (GGA) of Becke and Perdew for exchange and correlation functional (BPW91) was employed with the Martin (8s7p6d2f)/[6s5p3d2f] basis set[17]using the relativistic 19-electron Stuttgart−Dresden−Bonn (SDB) pseudopotentials.[18] The one-electron Darwin and mass-velocity relativistic corrections were included in this ECP. Frequency calculations and thermal energy corrections were performed at the same level of theory. The PES spectra were obtained by shifting the energy levels of occupied orbitals so that the highest occupied molecular orbital (HOMO) level was fit for VDE at a given calculation level.

To test the reliability of the calculation methods, we compared the calculated electronic properties of Au and Au_2 with experimental values. The electron affinity (EA) and ionization potential (IP) of a single Au atom at the B3LYP/HW [BPW91/HW] level are 2.17 [2.26] and 9.42 [9.50] eV, and those at the B3LYP/SDB [BPW91/SDB] level are 2.21 [2.25] and 9.43 [9.56] eV, respectively, These are in reasonable agreement with the experimental EA and IP (2.3 and 9.2 eV).[19] At the B3LYP/HW [BPW91/HW] level, the bond length and dissociation energy of Au_2 are estimated to be 2.57 [2.55] Å and 1.86 [2.03] eV, and at the B3LYP/SDB [BPW91/SDB] level those of Au_2 are 2.56 [2.54] Å and 1.92 [2.11] eV. These results are also in reasonable agreement with the experimental results, where the bond length and dissociation energy (D_0) of Au_2 are known to be 2.47 Å and 2.29 eV, respectively.[19]

We also employed MP2, CCSD, and CCSD(T) calculations. Both small HW and large SDB basis sets were used. All the MP2, CCSD, and CCSD(T) calculations were performed on the MP2/HW geometries. The BPW91/SDB results are similar to the B3LYP/HW results, and the MP2/SDB results are also similar to the MP2/HW results. Zero-point energy (ZPE) and thermal energy corrections were performed to obtain the ZPE-corrected interaction energy (ΔE_0) and free energy at 298 K and 1 atm (ΔG_{298}) at the B3LYP/HW and BPW91/SDB levels. Since the DFT results are found to be more consistent with experiment and are also closer to the CCSD and CCSD(T) results than the MP2 results, we discuss the DFT results unless otherwise specified.

However, we note that the MP2 and CCSD, CCSD(T) binding energies strongly depend on the basis set size. This indicates that even though the SDB basis set is not small, it still has large BSSEs. Thus, we carried out BSSEs using the counterpoise correction,[20] with which the total energies for 10 different structures composed of one real atom and the remaining nine dummy atoms were calculated, and the sum of them were subtracted by 10 times the energy of an isolated gold atom. In addition, to remove the finite size effect of basis sets used here, we estimated the complete basis set (CBS) limit value using the extrapolation (or partly interpolation) scheme that we previously reported.[21]

To demonstrate that the BSSE correction and the CBS extrapolation are meaningful not only for intermolecular interactions but also for strongly bound systems like the gold clusters, we calculated the binding energy of the gold dimer (Au_2) at the CCSD level using the HW and SDB basis sets, where the geometry was optimized at the CCSD/SDB level. The calculated bond length is 2.52 Å, comparable to the experimental value of 2.47 Å.[22] The binding energies are 1.80 and 1.96 eV for the HW and SDB basis sets, respectively, while the experimental value is 2.29 eV.[22] The estimated CBS limit value is 2.46 eV, which was closer to the experimental value. This demonstrates that the CBS estimation is reliable, and it is thus applicable to strongly bound systems like gold clusters. The extrapolation employed here is practically or to some extent an interpolation scheme as compared with other methods, which are solely extrapolations that do not give any proper bound values. It is true that the HW and SDB basis sets themselves give rather poor binding energies. In this regard, the CBS limit value is one of the alternatives to get more reliable binding energies for large systems like the gold decamer.

All the DFT and MP2 energy calculations were performed with the Gaussian suite of programs,[23] and all the CCSD and CCSD(T) calculations were performed with the MOLPRO package.[24] Charge and spin density were calculated with both the Gaussian[23] and VASP[25] programs. B3LYP/HW and BPW91/SDB calculations were carried out with atomic orbital basis sets. The plane wave calculations were carried out with the ultrasoft Vanderbilt pseudopotential and PW91 GGA exchange−correlation functional. Cluster structures were drawn with the Posmol package.[26]

III. Results and Discussion

A. Structures. To search for the lowest-energy structures for the neutral and anionic states of the gold decamer, we have carried out calculations for their various structures of different topologies at varied levels of theory. The low-lying energy structures of Au_{10} and Au_{10}^- are shown in Figure 1 and their relative energies, EAs, IPs, and VDEs are listed in Table 1, where we report only two competing 3D structures (3Da and 3Db) in the neutral state and three competing 3D structures (3Db, 3Dc, and 3Dd) in the anionic state, including the lowest-energy structures among several 3D structures at the MP2/SDB and BPW91/SDB levels.

For the low-lying 2D energy structures of Au_{10} with D_{3h}(triplet)_[111], C_{2v}, C_s, and D_{2h}_[100] symmetries (Figure 1a), where the crystal projection planes are given in brackets, the B3LYP/HW [BPW91/SDB] relative energies are 0.93 [0.82], 0.10 [0.57], 0.08 [0.19], and 0.00 [0.00] eV at 0 K, respectively, and 0.91 [0.79], 0.15 [0.62], 0.00 [0.11], and 0.01 [0.00] eV at 298 K, respectively. Thus, the temperature

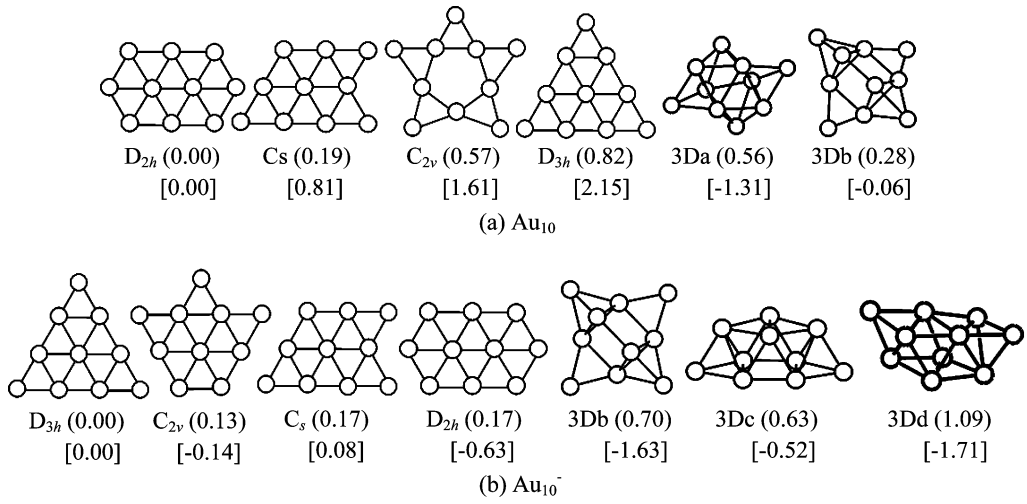

Figure 1. Various gold cluster structures with different topologies of (a) Au_{10} and (b) Au_{10}^-. BPW91/SDB [MP2/SDB] relative energies are in electronvolts in parentheses [brackets]. The given 3D structures are of the lowest energies among ~20 different 3D structures investigated here.

effect is very small, and the stability will be simply discussed based on 0 K. The corresponding MP2/HW [MP2/SDB] relative energies are 1.81 [2.15], 1.15 [1.61], 0.69 [0.81], and 0.00 [0.00] eV at 0 K, respectively. DFT and MP2 calculations are consistent, but the MP2 calculations stabilize the D_{2h} structure more.

As for Au_{10}^-, the B3LYP/HW [BPW91/SDB] relative energies of the D_{3h}_(triplet), C_{2v}, C_s, and D_{2h} structures (Figure 1b) are 0.00 [0.00], 0.04 [0.13], 0.08 [0.17], and 0.24 [0.17] eV at 0 K, respectively, and 0.00 [0.00], 0.03 [0.12], 0.07 [0.18], and 0.27 [0.20] eV at 298 K, respectively. Thus, the temperature effect is again very small. The corresponding MP2/HW [MP2/SDB] relative energies are 0.00 [0.00], −0.10 [−0.14], 0.04 [0.08], and −0.55 [−0.63] eV, respectively. Thus, in the case of Au_{10}^-, the ordering of relative energies for the above four clusters is completely reversed between the DFT and MP2 results.

On metal clusters like Au_8, we note that, as compared with the MP2 results, the DFT results are more consistent with very accurate calculations such as CCSD(T), while the CCSD results are almost in between the DFT and MP2 results.[27] Nevertheless, in consideration that DFT often fails in properly describing anionic clusters, we have carried out CCSD//MP2 calculations using both the HW and SDB ECPs. The CCSD results for Au_{10}^- show that the D_{3h} structure is 0.04 eV more stable than the D_{2h} structure, which is more consistent with the DFT results. Therefore, even for the anionic gold clusters, the DFT results are more reliable than the MP2 results. This will be further verified by the electronic properties and PES spectra, which will be discussed later.

At the B3LYP/HW [BPW91/SDB] level, the 2D structures are favored for both neutral and anionic states; the 3D lowest-energy structure is 0.09/0.53 [0.28/0.63] eV higher than the 2D lowest-energy structure in the neutral/anionic state. However, at the MP2/HW [MP2/SDB] level, the 3D structures are favored for both neutral and anionic states; the 3D lowest-energy neutral/anionic structure is 1.11/0.89 [1.31/1.08] eV more stable than the 2D lowest-energy neutral(D_{2h})/anionic(D_{3h}) structure. It is well-known that, in cluster calculations, MP2 results tend to favor 3D structures over 2D structures, while DFT results are often in favor of 2D structures.[28] On the other hand, in the CCSD/HW [CCSD/SDB] calculations of the neutral state, the 3D structure is [0.70/0.30] eV more stable than the 2D D_{2h} structure. In the CCSD/HW calculations of the anionic state, the 3D structure is 0.58 eV more stable than the 2D D_{3h} structure, whereas the 2D D_{3h} structure is 0.97 eV more stable than the 3D structure in the CCSD/SDB calculations. For the CCSD(T)/HW calculations of the neutral/anionic state, the 3D structure is 0.91 and 0.87 eV more stable than the 2D D_{2h}/D_{3h} structure.

However, the 3D structures tend to have larger BSSEs than 2D structures, so we have done the BSSE correction for the 2D and 3D lowest-energy structures at the CCSD and CCSD(T) levels. The stabilities for 2D and 3D structures of neutral and anionic states are reversed after the BSSE correction except for the structures of anionic states at the CCSD/SDB level. The 2D lowest-energy neutral(D_{2h})/anionic(D_{3h}) structure is 0.18/0.32 [0.01/0.07] eV more stable than the 3D lowest-energy structure at the CCSD/HW [CCSD(T)/HW] level and 0.31/1.24 eV more stable than the 3D structure at the CCSD/SDB level.

We also estimated the CBS limit value. In the case of neutral state, the BSSE corrected and uncorrected energies for the two different HW and SDB basis sets were used to estimate the CCSD/CBS value. Then, the neutral/anionic 2D structure is 0.60/1.63 eV more stable than the 3D lowest-energy structure. The BSSE uncorrected [corrected] relative energy of the anionic 2D D_{3h} structure with respect to the 3D lowest-energy structure (3Dc) is 0.58 [−0.32] eV, whereas that of the neutral 2D D_{2h} structure is 0.70 [−0.18] eV.

Thus, the BSSE correction enhances the stability of anionic/neutral 2D structure over the 3D structure by 0.90/0.88 eV, which indicates that the BSSE correction effect is almost the same for both anionic and neutral systems. Since the BSSEs for MP2, CCSD, and CCSD(T) calculations are similar in most cases, in the neutral [anionic] state the relative

Table 1. Relative Binding Energies, Vertical Electron Affinities, Vertical Ionization Potentials, and Vertical Detachment Energies of Au_{10} and Au_{10}^- [a]

Au_{10}: ΔE_0 (ΔG_{298})	$D_{3h}^{(t)}$	C_{2v}	C_s	D_{2h}	3Da	3Db
B3LYP/HW	0.93 (0.91)	0.10 (0.15)	0.08 (0.00)	0.00 (0.01)	0.59 (0.60)	0.09 (0.05)
BPW91/SDB	0.82 (0.79)	0.57 (0.62)	0.19 (0.11)	0.00 (0.00)	0.56 (0.58)	0.28 (0.24)
MP2/HW	1.81	1.15	0.69	0.00	−1.11	−0.08
MP2/SDB	2.15	1.61	0.81	0.00	−1.31	−0.06
CCSD/HW				0.00	−0.70	−0.31
CCSD/HW-BSSE				0.00	0.18	0.28
CCSD/SDB				0.00	−0.30	
CCSD/SDB-BSSE				0.00	0.31	
CCSD/CBS				0.00	0.60	
CCSD(T)/HW				0.00	−0.91	−0.27
CCSD(T)/HW-BSSE				0.00	0.01	0.34
CCSD(T)/CBS				0.00	0.43	

Au_{10}^-: ΔE_0 (ΔG_{298})	D_{3h}	C_{2v}	C_s	D_{2h}	3Db	3Dc	3Dd
B3LYP/HW	0.00 (0.00)	0.04 (0.03)	0.08 (0.07)	0.24 (0.27)	0.53 (0.52)	0.75 (0.76)	1.10 (1.07)
BPW91/SDB	0.00 (0.00)	0.13 (0.12)	0.17 (0.18)	0.17 (0.20)	0.63 (0.62)	0.70 (0.71)	1.09 (1.07)
MP2/HW	0.00	−0.10	0.04	−0.55	−0.39	−1.35	−1.44
MP2/SDB	0.00	−0.14	0.08	−0.63	−0.52	−1.63	−1.71
CCSD/HW	0.00			0.04	−0.08	−0.58	0.27
CCSD/HW-BSSE	0.00					0.32	
CCSD/SDB	0.00					0.97	
CCSD/SDB-BSSE	0.00					1.24	
CCSD/CBS	0.00					1.63	
CCSD(T)/HW	0.00				−0.17	−0.87	
CCSD(T)/HW-BSSE	0.00					0.07	
CCSD(T)/CBS	0.00					1.38	

Au_{10}: EA_v	$D_{3h}^{(t)}$	C_{2v}	C_s	D_{2h}	3Da	3Db
B3LYP/HW	4.01	3.09	3.06	2.82	2.47	2.54
BPW91/SDB	3.75	3.19	2.72	2.76		

Au_{10}: IP_v	$D_{3h}^{(t)}$	C_{2v}	C_s	D_{2h}	3Da	3Db
B3LYP/HW	7.59	8.07	7.50	7.70	7.26	7.11
BPW91/SDB	7.51	7.42	7.31	7.48	7.23	7.04
MP2/HW	6.88	7.23	7.02	7.52	6.92	6.61
MP2/SDB	7.58	8.66	7.98	8.15	7.79	7.63
CCSD/HW				7.05	6.61	6.38

Au_{10}^-: VDE	D_{3h}	C_{2v}	C_s	D_{2h}	3Db	3Dc	3Dd
B3LYP/HW	4.17	3.55	3.26	3.02	3.22	2.90	2.83
BPW91/SDB	3.98	3.50	3.13	2.93	3.06	2.84	2.62
MP2/HW	3.76		2.59	2.49	2.59	2.36	2.58
MP2/SDB	4.24	3.78	3.23	3.08	3.20	3.02	3.18
CCSD/HW	3.53				2.63	2.27	1.74
CCSD(T)/HW	3.64				2.72	2.44	

[a] Values in parentheses are the relative free energies at room temperature and 1 atm (ΔG_{298}); otherwise, values denote the zero-point-energy-corrected relative energy (ΔE_0). The experimental IP of Au_{10} is 8.2 eV and photoelectron spectra show small peaks around 2.9−3.5 eV and main peaks around 4.0 eV.[14,15] Superscript (t) indicates the triplet spin state, and suffix -BSSE indicates the BSSE-corrected relative energy. See text for estimation of the CBS energy.

energy of the 3Da [3Dc] structure at the CCSD(T)/HW level is likely to be 0.17 [0.25] eV lower than that at the CCSD/HW level. Thus, at the CCSD(T)/CBS level, the neutral and anionic 2D structures are 0.43 and 1.38 eV more stable than the corresponding 3D structures, respectively. This indicates that both neutral and anionic Au_{10} have the 2D structures, which will be further verified by comparing the predicted IP and VDE with the experimental data.

B. Ionization Potential and Vertical Detachment Energy. It is noted that the IPs are underestimated at the B3LYP/HW, BPW91/SDB, and MP2 levels. In the case of Au_8,[7] the experimental IP is 8.65 eV, while the predicted IP at the B3LYP/HW [BPW91/SDB] level is 8.11 [8.03] eV, which is underestimated by 0.54 [0.62] eV. Thus, the predicted IP at this level of theory is underestimated. On the other hand, the predicted VDEs are in good agreement with experiments. For Au_8^-,[8] the predicted VDE is 2.94 eV, in good agreement with the experimental VDE of 2.79 eV. In this regard, the VDE is the useful information to find the right structure.

The IPs of 2D D_{2h} and 3Da structures of Au_{10} are estimated to be 7.70 [7.48, 7.49] and 7.26 [7.23, 7.07] eV at the B3LYP/HW [BPW91/SDB, B3LYP/SDB] level and 7.49 [7.24] eV at the B3LYP/SDB level, while the experimental

IP of Au_{10} is known to be 8.2 eV.[14,15] Thus, in the case of 3D structure, the predicted IPs are underestimated by 0.94 [0.97] eV at the B3LYP/HW [BPW91/SDB] level, whereas in the case of 2D structure, the predicted IPs are underestimated by 0.50 [0.72] eV at the B3LYP/HW [BPW91/SDB] level. In addition, the IPs of 2D D_{2h} and 3Da structures are 7.52 [8.15] and 6.92 [7.79] eV at the MP2/HW [MP2/SDB] level, respectively. Thus, the MP2/SDB IP of 2D D_{2h} (8.15 eV) agrees well with the experimental value (8.2 eV). Nevertheless, the corresponding values for CCSD(HW) are 7.05 and 6.61 eV, in poor agreement, possibly due to the insufficient basis set at the CCSD level. As the long-range dispersion effect such as aurophilic effects[29] would be important in the gold systems, the DFT IPs would be underestimated. Nevertheless, it is not clear only from the present data because we were not able to obtain the IPs at the CCSD(T) level using a large basis set. The available data imply that the IPs for 2D structure lie in a more probable range than the 3D structure. This could indicate that the lowest-energy structure of neutral Au_{10} is likely to be 2D D_{2h}. On the other hand, the calculated B3LYP/HW [BPW91/SDB] PES spectra of Au_{10}^- isomers match the experimental[8,14,15] ones. The experimental PES spectrum of Au_{10}^- shows small peaks from 2.9 to 3.5 eV, which correspond to the predicted isomers of C_{2v} (3.55 [3.50] eV), C_s (3.26 [3.13] eV), and D_{2h} (3.02 [2.93] eV) structures, while the main peaks around 4.0 eV correspond to the minimum-energy isomer having the D_{3h} (4.17 [3.98] eV) structure. Moreover, the relative intensities of the experimental PES peaks, which reflect the populations of the given clusters, indicate that the 2D structure with D_{3h} symmetry would be the lowest-energy structure of Au_{10}^-. None of the low-energy 3D anionic structures matches the experimental VDE.

C. Origin of Stability and Large Vertical Detachment Energy. To understand why the 2D structures are more stable than the 3D structures in both neutral and anionic states, we investigate the same planar D_{2h} structures of Au_{10}_D_{2h}, Ag_{10}_D_{2h}, and Na_{10}_D_{2h} by carrying out the BPW91/SDB calculations for Au_{10} and Ag_{10}, and the BPW91/cc-pCVDZ calculations for Na_{10} (as the SDB basis set is not available for Na). The total charges on the six apex atoms of Au_{10}_D_{2h}, Ag_{10}_D_{2h}, and Na_{10}_D_{2h} are −0.21, −0.15, and −0.15, respectively. Their charge populations of s/p/d orbitals of the HOMO state are 0.74/0.02/0.24, 0.77/0.17/0.06, and 0.79/0.21/0.00, respectively. The apex atoms of Au_{10}_D_{2h} have a significant charge population of d orbitals in contrast to those of Na_{10}_D_{2h}, which have a significant population of p orbitals. For Au_{10}_D_{2h}, the charge repulsions become minimal because the distances between different apexes are much more separated than the distances between any other sites. This demonstrates that the near-degeneracy (driven by relativistic effects) of 6s and 5d orbitals plays an important role in stabilizing 2D Au clusters, which is almost absent in Na and Ag. We also investigated the same planar triangular structures of Au_{10}^-_D_{3h}, Ag_{10}^-_D_{3h}, and Na_{10}^-_D_{3h}. The charges of an apex atom for Au_{10}^-_D_{3h}, Ag_{10}^-_D_{3h}, and Na_{10}^-_D_{3h} are −0.29, −0.25, and −0.25, respectively. Their charge populations of s/p/d orbitals of the singly occupied molecular orbital (SOMO) states are 0.68/0.02/0.30, 0.75/0.18/0.07, and 0.82/0.18/0.00, respectively, which also shows the near-degeneracy (driven by relativistic effects) of 6s and 5d orbitals. In Au_{10}^-_D_{3h}, the excess electron is also mostly populated on the apex atoms in the triangular structure. Since the Coulombic repulsions between apex atoms (which are more separated than any other two atoms) are weaker, this energy gain makes the 2D D_{3h} structure more stabilized than other structures, which would result in lowering the SOMO energy and hence increasing VDE.

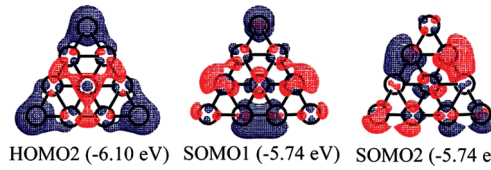

Figure 2. Frontier molecular orbitals of Au_{10}_D_{3h} at the BPW91/SDB level. The orbital energy is given in parentheses.

Figure 2 shows the molecular orbital of Au_{10} at the BPW91/SDB level. Au_{10}^- is predicted to have a small energy separation (less than 0.1 eV) between the first and second PES peaks, in agreement with the experimental PES of Au_{10}^-.[8,14] This reflects why the ground-state neutral structure (D_{3h}) of Au_{10}, which has the same triangular geometry with the lowest-energy structure (D_{3h}) of anionic Au_{10}^-, is a triplet. A large vertical electron affinity (EA_v) of the neutral structure Au_{10}_D_{3h} is due to two degenerate low-energy SOMOs. Since an additional electron occupies one of the two low-energy SOMOs, Au_{10}^- has a large VDE in contrast to the case when the electron occupies the lowest unoccupied molecular orbital (LUMO). Thus, the VDE of Au_{10}^- is large, unlike other ordinary even-numbered gold clusters whose VDEs are small. Though Au_{10}^- maintains a triangular structure, its symmetry changes from D_{3h} to C_{2v}^{JT} (though very close to D_{3h}) for better stabilization due to the Jahn−Teller (JT) distortion.

D. Charge−Spin Separation. Natural bond orbital (NBO) charges (Q) and spin populations (S) in Au_{10} and Au_{10}^- calculated at the BPW91/SDB level are in Table 2. An excess electron can go into one of the doubly degenerate SOMO levels of Au_{10}_D_{3h} with equal probabilities. The charge of an edge atom is either positive (i.e., electron-deficient; 0.07 for Au_{10}_D_{3h}) or nearly zero (−0.01 for Au_{10}^-_C_{2v}^{JT}), while the charge of an apex atom is highly negative (−0.13 au for Au_{10}_D_{3h} and −0.29 au for Au_{10}^-_C_{2v}^{JT}). Charge density is separated into regions with either positively or minimally negatively charged edges and regions with highly negatively charged apexes, which results in maximizing the electrostatic energy gain.

Here, we note a fascinating phenomenon in Au_{10}_D_{3h} and Au_{10}^-_C_{2v}^{JT}, whose spin density is small around the central and apex atoms but high around edge atoms, as shown in Table 2. Thus, the spin density is populated almost oppositely to the charge density. To verify these results, we also performed charge and spin density calculations using the plane wave pseudopotential methods (instead of the Gaussian type orbital methods) with generalized gradient approximation to exchange−correlation using the VASP package. These charge and spin densities (Figure 3) are consistent with those based on BPW91/SDB with the Gaussian orbitals (Table 2).

Table 2. Charge and Spin of Each Type of Atom for Six Triangular Structures[a]

	$Au_{10}^-\_C_{2v}^{JT}$		$Au_{10}^{(t)}\_D_{3h}$		$Na_{10}^{(t)}\_D_{3h}$		$Ag_{10}^{(t)}\_D_{3h}$		$Pt_{10}^{(s)}\_C_{2v}$		$Au_{15}^{(d)}\_C_{2v}$	
atoms	*Q*	*S*	*Q*	*S*	*Q*	*S*	*Q*	*S*	*Q*	*S*	*Q*	*S*
center	0.01	0.11	−0.03	0.16	−0.25	−0.10	−0.19	−0.02	−0.12	0.18	0.01	0.05
edge	−0.02	0.12	0.07	0.24	0.07	0.25	0.07	0.23	0.09	0.58	0.04	0.04
apex	−0.29	0.06	−0.13	0.14	−0.05	0.20	−0.07	0.20	−0.13	0.78	−0.14	0.16

[a] Charge (*Q*) and spin (*S*) are given in atomic units. Superscripts (t), (s), and (d) denote triplet, septet, and doublet spin states, respectively, and subscript JT denote the Jahn−Teller distortion. C_{2v}^{JT} is very close in structure to D_{3h}. $Au_{10}^-\_C_{2v}^{JT}$, $Au_{10}^{(t)}\_D_{3h}$, $Ag_{10}^{(t)}\_C_{2v}$, $Pt_{10}^{(s)}\_C_{2v}$, and $Au_{15}^{(d)}\_C_{2v}$ were calculated at the BPW91/SDB level and $Na_{10}^{(t)}\_D_{3h}$ was calculated at the BPW91/cc-pCVDZ level.

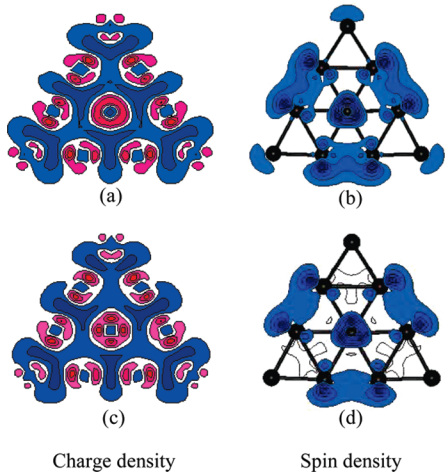

Figure 3. Charge density and spin density for (a, b) $Au_{10}\_D_{3h}$ and (c, d) $Au_{10}^-\_C_{2v}^{JT}$ (which is similar to D_{3h}). The difference of the total charge density from the sum of charge densities of all isolated gold atoms at each position of Au_{10} is plotted in contour map, based on the plane wave DFT calculations, where blue indicates regions with rich electron or spin density, while red indicates regions with depleted electron density.

The spin densities arise mainly from frontier singly occupied orbitals. For $Au_{10}\_D_{3h}$, both SOMOs (SOMO1 and SOMO2) are mainly distributed around the edge atoms, resulting in larger spin density on the edge atoms. On the other hand, the charge density is mostly populated around the apex atoms because of the doubly occupied molecular orbitals below SOMOs. Therefore, we note the substantial SCSS, which is extremely rare. When an excess electron is added to $Au_{10}\_D_{3h}$, it occupies one of the SOMOs; thus the total spin of $Au_{10}^-\_D_{3h}$ (which eventually changes to $Au_{10}^-\_C_{2v}^{JT}$ due to the JT effect) is reduced from 2 to 1, partly suppressing the spin density. Nevertheless, the SCSS is still clear in $Au_{10}^-\_D_{3h}$ and $Au_{10}^-\_C_{2v}^{JT}$.

By including spin−orbit coupling, magnetization was evaluated for the neutral-state 2D D_{3h} structure using plain wave pseudopotential density functional methods. The average magnetization per atom on the apex atoms is only 4.6% of total magnetization, while that on the edge atoms is 11.3%, and the unoccupied states are located in a very low energy region only 0.25 eV higher than the occupied states, which shows that even though the spin−orbit coupling is included, the characteristic electronic structures for the 2D D_{3h} structure are maintained.

For comparison, we investigated the planar structures of Au_{10} clusters with D_{2h}, C_s, and C_{2v} symmetries shown in Figure 1. These do not show SCSS because these lowest-energy spin states are singlet states. Planar triangular $Au_6\_D_{3h}$ and $Au_{15}\_D_{3h}$ were also investigated to verify whether planar triangular symmetry is the necessary condition for SCSS. $Au_6\_D_{3h}$ has a singlet spin state, resulting in no SCSS, while $Au_{15}\_D_{3h}$ has a doublet spin state with large densities of both charge and spin on apex atoms and does not show unusual SCSS because the charge goes with the spin (Table 2). This indicates that the degenerate triplet state of 10 metal atoms cluster with planar triangular D_{3h} symmetry results in substantial SCSS. In this regard, we studied other metal systems with planar triangular structures of $Ag_{10}\_D_{3h}$ and $Na_{10}\_D_{3h}$, which satisfy the conditions for SCSS as mentioned above. They also showed SCSS, though less than $Au_{10}\_D_{3h}$, as shown in Table 2. We also investigated planar triangular $Pt_{10}\_D_{3h}$ (or $Pt_{10}\_C_{2v}^{JT}$). This is slightly distorted to have C_{2v} symmetry, still maintaining the triangular geometry. In contrast to $Ag_{10}\_D_{3h}$ and $Na_{10}\_D_{3h}$, which show significant SCSS (though less than $Au_{10}\_D_{3h}$), $Pt_{10}\_C_{2v}^{JT}$ (which has almost the same planar triangular geometry as $Au_{10}\_D_{3h}$) has different electronic configurations and a different spin state (septet) from $Au_{10}\_D_{3h}$. It shows both large charge and spin densities on apex atoms but no significant SCSS. Though $Ag_{10}\_D_{3h}$ and $Na_{10}\_D_{3h}$ show some SCSS, these clusters can hardly be made because they are much less stable than the global minimum-energy structure, while $Au_{10}\_D_{3h}$ can be synthesized by detaching one electron from the experimentally identified lowest-energy structure $Au_{10}^-\_D_{3h}$.

As shown in $Au_{10}^-\_D_{3h}$, this kind of spin polarization is called s-electron ferromagnetism,[30] where several degenerate HOMO levels due to highly symmetric geometry are partially occupied with s electrons whose spins are aligned according to Hund's rule. Therefore, such s-electron ferromagnetism is realized in the planar $Au_{10}\_D_{3h}$ cluster, while in this case the nearly degenerate d-orbitals also play a role in enhancing the ferromagnetism. Moreover, the spin on planar $Au_{10}\_D_{3h}$ would not be seriously influenced by surrounding environments, because its spin is mainly distributed around edge atoms due to SCSS, suggesting a possible use of the $Au_{10}\_D_{3h}$ cluster as a spin quantum dot.

IV. Conclusion

For gold clusters, the near-degeneracy (driven by relativistic effects) of 5d and 6s orbitals helps stabilize acute apex gold atoms. Thus, small gold clusters tend to have planar structures, and the transition from 2D to 3D structural transformation is considered to be around decamers. For Au_{10} and Au_{10}^-, DFT (B3LYP/HW and PBW91/SDB) predicts 2D structures, while MP2 (MP2/HW and MP2/SDB) predicts 3D structures. At the CCSD/HW and CCSD(T)/HW levels

of theory, Au_{10} and Au_{10}^- are also predicted to have 3D structures; at the CCSD/SDB level, Au_{10} favors 3D, while Au_{10}^- favors 2D. However, according to the estimated CCSD(T)/CBS limit with the BSSE correction, it is predicted that both Au_{10} and Au_{10}^- favor 2D structures.

The VDEs of the 2D anionic gold decamer isomers studied here explain a few peaks in the experimental PES spectra, while the $Au_{10}^-\_D_{3h}$ VDE peak is clearly dominant. Upon binding an excess electron, the degenerate state of D_{3h} symmetry transforms Au_{10}^- into a structure of C_{2v} symmetry due to the JT distortion. The calculated VDE for $Au_{10}^-\_C_{2v}^{JT}$ (close to D_{3h} symmetry) is in good agreement with the experimental value, while the VDEs of competing structures agree with a few minor peaks in the experimental PES spectra. The unusual small separation between the first and second peaks in the PES is found to be due to the doubly degenerate low-energy SOMOs of $Au_{10}^-\_D_{3h}$. Though even-numbered gold clusters usually have small VDE, $Au_{10}^-\_D_{3h}$ shows relatively large VDE due to the same reason. $Au_{10}\_D_{3h}$ and $Au_{10}^-\_C_{2v}^{JT}$ shows s-electron ferromagnetism and remarkable spatial charge-spin separations, which could be useful in spintronics.[31]

Acknowledgment. This work was supported by the projects supported by GRL/KICOS, KOSEF (WCU, R32-2008-000-10180-0, and EPB Center, R11-2008-052-01000), BK21, and KRF-2006-353-C00022 (MOEHRD) and KISTI (KSC-2008-K08-0002 and KSC-2007-S00-3005).

References

(1) (a) Häkkinen, H.; Moseler, M.; Landman, U. *Phys. Rev. Lett.* **2002**, *89*, 033401. (b) Pyykkö, P. *Angew. Chem., Int. Ed.* **2002**, *41*, 2174. (c) Böhme, D. K.; Schwarz, H. *Angew. Chem., Int. Ed.* **2005**, *44*, 2336. (d) Wesendrup, R.; Hunt, T.; Schwerdtfeger, P. *J. Chem. Phys.* **2000**, *112*, 9356. (e) Yoon, J.; Kim, K. S.; Baeck, K. K. *J. Chem. Phys.* **2000**, *112*, 9335. (f) Zheng, J.; Petty, J. T.; Dickson, R. M. *J. Am. Chem. Soc.* **2003**, *125*, 7780. (g) Pyykkö, P. *Nat. Nanotechnol.* **2007**, *2*, 273.

(2) (a) Barnett, R. N.; Landman, U. *Nature (London)* **1997**, *387*, 788. (b) Häkkinen, H.; Barnett, R. N.; Landman, U. *J. Phys. Chem. B* **1999**, *102*, 8814. (c) Rodrigues, V.; Fuhrer, T.; Ugarte, D. *Phys. Rev. Lett.* **2000**, *85*, 4124. (d) Hong, B. H.; Bae, S. C.; Lee, C.; Jeong, S.; Kim, K. S. *Science* **2001**, *294*, 348. (e) Rodrigues, V.; Bettini, J.; Silva, P. C.; Ugarte, D. *Phys. Rev. Lett.* **2003**, *91*, 096801. (f) Geng, W. T.; Kim, K. S. *Phys. Rev. B* **2003**, *67*, 233403. (g) Nautiyal, T.; Rho, T. H.; Kim, K. S. *Phys. Rev. B* **2004**, *69*, 193404. (h) Lee, Y.-J.; Brandbyge, M.; Puska, M. J.; Taylor, J.; Stokbro, K.; Nieminen, R. M. *Phys. Rev. B* **2004**, *69*, 125409. (i) Cheng, D. Y.; Kim, W. Y.; Min, S. K.; Nautiyal, T.; Kim, K. S. *Phys. Rev. Lett.* **2006**, *96*, 096104. (j) Han, Y.-K.; Jung, J. *J. Chem. Phys.* **2006**, *125*, 084101.

(3) (a) Kim, W. Y.; Choi, Y. C.; Kim, K. S. *J. Mater. Chem.* **2008**, *18*, 4510. (b) Singh, N. J.; Lee, E. C.; Choi, Y. C.; Lee, H. M.; Kim, K. S. *Bull. Chem. Soc. Jpn.* **2007**, *80*, 1437.

(4) (a) Pyykkö, P. *Chem. Rev.* **1988**, *88*, 563. (b) Schwerdtfeger, P.; Dolg, M.; Schwarz, W. H. E.; Bowmaker, G. A.; Boyd, P. D. W. *J. Chem. Phys.* **1989**, *91*, 1762. (c) Pyykkö, P. *Angew. Chem., Int. Ed.* **2002**, *41*, 3573. (d) Nautiyal, T.; Youn, S. J.; Kim, K. S. *Phys. Rev. B* **2003**, *68*, 033407. (e) Choi, Y. C.; Lee, H. M.; Kim, W. Y.; Kwon, S. K.; Nautiyal, T.; Cheng, D. Y.; Vishwanathan, K.; Kim, K. S. *Phys. Rev. Lett.* **2007**, *98*, 076101.

(5) (a) Li, J.; Li, X.; Zhai, H.; Wang, L.-S. *Science* **2003**, *299*, 864. (b) Schwerdtfeger, P. *Angew. Chem., Int. Ed.* **2003**, *42*, 1892. (c) Bonacic-Koutecky, V.; Burda, J.; Mitric, R.; Ge, M.; Zampella, G.; Fantucci, P. *J. Chem. Phys.* **2002**, *117*, 3120. (d) Pyykkö, P. *Angew. Chem., Int. Ed.* **2004**, *43*, 4412. (e) Yoon, B.; Häkkinen, H.; Landman, U.; Worz, A. S.; Antonietti, J.-M.; Abbet, S.; Judai, K.; Heiz, U. *Science* **2005**, *307*, 403. (f) Olson, R. M.; Varganov, S.; Gordon, M. S.; Metiu, H.; Chretien, S.; Piecuch, P.; Kowalski, K.; Kucharski, S. A.; Musial, M. *J. Am. Chem. Soc.* **2005**, *127*, 1049. (g) Lee, H. M.; Diefenbach, M.; Suh, S. B.; Tarakeshwar, P.; Kim, K. S. *J. Chem. Phys.* **2005**, *123*, 743281. (h) Walker, A. V. *J. Chem. Phys.* **2005**, *122*, 943101. (i) Remacle, F.; Kryachko, E. S. *J. Chem. Phys.* **2005**, *122*, 443041. (j) Gronbeck, H.; Broqvist, P. *Phys. Rev. B* **2005**, *71*, 734081. (k) Ji, M.; Gu, X.; Li, X.; Gong, X. G.; Li, J.; Wang, L.-S. *Angew. Chem., Int. Ed.* **2005**, *44*, 7119. (l) Ricci, D.; Bongiorno, A.; Pacchioni, G.; Landman, U. *Phys. Rev. Lett.* **2006**, *97*, 036106. (m) Han, Y.-K. *J. Chem. Phys.* **2006**, *124*, 243161. (n) Bulusu, S.; Li, X.; Wang, L. S.; Zeng, X. C. *Proc. Natl. Acad. Sci. U.S.A.* **2006**, *103*, 8326. (o) Bulusu, S.; Li, X.; Wang, L.-S.; Zeng, X. C. *J. Phys. Chem. C* **2007**, *111*, 4190.

(6) (a) Lee, Y. S.; Ermler, W. C.; Pitzer, K. S.; McLean, A. D. *J. Chem. Phys.* **1979**, *70*, 288. (b) Ermler, W. C.; Lee, Y. S.; Pitzer, K. S. *J. Chem. Phys.* **1979**, *70*, 293. (c) Ziegler, T.; Snijders, J. G.; Baerends, E. J. *Chem. Phys. Lett.* **1980**, *75*, 1. (d) Ziegler, T.; Snijders, J. G.; Baerends, E. J. *J. Chem. Phys.* **1981**, *74*, 1271. (e) Lee, H.-S.; Han, Y-K.; Kim, M. C.; Bae, C.; Lee, Y. S. *Chem. Phys. Lett.* **1998**, *293*, 97. (f) Pyykkö, P.; Zhao, Y. *Angew. Chem., Int. Ed.* **1991**, *30*, 604. (g) Li, J.; Pyykkö, P. *Chem. Phys. Lett.* **1992**, *197*, 586. (h) Häkkinen, H. *Chem. Soc. Rev.* **2008**, *37*, 1847.

(7) Lee, H. M.; Ge, M.; Sahu, B. R.; Tarakeshwar, P.; Kim, K. S. *J. Phys. Chem. B* **2003**, *107*, 9994.

(8) Häkkinen, H.; Yoon, B.; Landman, U.; Li, X.; Zhai, H.; Wang, L.-S. *J. Phys. Chem. A* **2003**, *107*, 6168.

(9) Häkkinen, H.; Abbet, S.; Sanshez, A.; Heiz, U.; Landman, U. *Angew. Chem., Int. Ed.* **2003**, *42*, 1297.

(10) (a) Wang, J.; Wang, G.; Zhao, J. *Phys. Rev. B* **2002**, *66*, 035418. (b) Häkkinen, H.; Landman, U. *Phys. Rev. B* **2000**, *62*, R2287. (c) Soulé de Bas, B.; Ford, M. J.; Cortie, M. B. *J. Mol. Struct. (THEOCHEM)* **2004**, *686*, 193.

(11) Furche, F.; Ahlrichs, R.; Weis, P.; Jacob, C.; Gilb, S.; Bierweiler, T.; Kappes, M. M. *J. Chem. Phys.* **2002**, *117*, 6982.

(12) Gilb, S.; Jacobsen, K.; Schooss, D.; Furche, F.; Ahlrichs, R.; Kappes, M. M. *J. Chem. Phys.* **2004**, *121*, 4619.

(13) (a) Wells, D. H., Jr.; Delgass, W. N.; Thomson, K. T. *J. Chem. Phys.* **2002**, *117*, 10597. (b) Weis, P. *Int. J. Mass Spectrom.* **2005**, *245*, 1.

(14) Taylor, K. J.; Pettiette-Hall, C. L.; Cheshnovski, O.; Smalley, R. E. *J. Chem. Phys.* **1992**, *96*, 3319.

(15) (a) Chesnovsky, O.; Pettiette, C. L.; Smalley, R. E. *Ion and Cluster Ion Spectroscopy and Structure*; Maier, J. P., Ed.; Elsevier: Amsterdam, 1988. (b) Jackschath, C.; Rabin, I.; Schulze, W. *Ber. Bunsen-Ges. Phys. Chem.* **1992**, *96*, 1200.

(16) Hay, P. J.; Wadt, W. R. *J. Chem. Phys.* **1985**, *82*, 299.

(17) Martin, J. M. L.; Sundermann, A. *J. Chem. Phys.* **2001**, *114*, 3408.

(18) Andrae, D.; Haeussermann, U.; Dolg, M.; Stoll, H.; Preuss, H. *Theor. Chim. Acta* **1990**, *77*, 123.

(19) (a) Bishea, G. A.; Morse, M. D. *J. Chem. Phys.* **1991**, *95*, 5646. (b) Huber, K. P.; Herzberg, G. *Constants of Diatomic Molecules*; Van Nostrand Reinhold: New York, 1979. (c) Bauschlicher, C. W., Jr.; Langhoff, S. R.; Partridge, H. *J. Chem. Phys.* **1989**, *91*, 2412.

(20) Boys, S. F.; Bernardi, F. *Mol. Phys.* **1970**, *19*, 533.

(21) Min, S. K.; Lee, E. C.; Lee, H. M.; Kim, D. Y.; Kim, D.; Kim, K. S. *J. Comput. Chem.* **2008**, *29*, 1208.

(22) (a) Hilpert, K.; Gingerich, K. A. *Ber. Bunsen-Ges. Phys. Chem.* **1980**, *84*, 739. (b) Smard, B.; Hackett, P. A. *J. Mol. Spectrosc.* **1990**, *142*, 310.

(23) Frisch, M. J. ; Trucks, G. W.; Schlegel, H. B.; Scuseria, G. E.; Robb, M. A.; Cheeseman, J. R.; Montgomery, J. A., Jr.; Vreven, T.; Kudin, K. N.; Burant, J. C.; Millam, J. M.; Iyengar, S. S.; Tomasi, J.; Barone, V.; Mennucci, B.; Cossi, M.; Scalmani, G.; Rega, N.; Petersson, G. A.; Nakatsuji, H.; Hada, M.; Ehara, M.; Toyota, K.; Fukuda, R.; Hasegawa, J.; Ishida, M.; Nakajima, T.; Honda, Y.; Kitao, O.; Nakai, H.; Klene, M.; Li, X.; Knox, J. E.; Hratchian, H. P.; Cross, J. B.; Bakken, V.; Adamo, C.; Jaramillo, J.; Gomperts, R.; Stratmann, R. E.; Yazyev, O.; Austin, A. J.; Cammi, R.; Pomelli, C.; Ochterski, J. W.; Ayala, P. Y.; Morokuma, K.; Voth, G. A.; Salvador, P.; Dannenberg, J. J.; Zakrzewski, V. G.; Dapprich, S.; Daniels, A. D.; Strain, M. C.; Farkas, O.; Malick, D. K.; Rabuck, A. D.; Raghavachari, K.; Foresman, J. B.; Ortiz, J. V.; Cui, Q.; Baboul, A. G.; Clifford, S.; Cioslowski, J.; Stefanov, B. B.; Liu, G.; Liashenko, A.; Piskorz, P.; Komaromi, I.; Martin, R. L.; Fox, D. J.; Keith, T.; Al-Laham, M. A.; Peng, C. Y.; Nanayakkara, A.; Challacombe, M.; Gill, P. M. W.; Johnson, B.; Chen, W.; Wong, M. W.; Gonzalez, C.; Pople, J. A. Gaussian 03, Revision C.02; Gaussian, Inc., Wallingford, CT, 2004.

(24) Werner, H.-J.; Knowles, P. J.; Lindh, R.; Manby, F. R.; Schütz, M.; Celani, P.; Korona, T.; Mitrushenkov, A.; Rauhut, G.; Adler, T. B.; Amos, R. D.; Bernhardsson, A.; Berning, A.; Cooper, D. L.; Deegan, M. J. O.; Dobbyn, A. J.; Eckert, F.; Goll, E.; Hampel, C.; Hetzer, G.; Hrenar, T.; Knizia, G.; Köppl, C.; Liu, Y.; Lloyd, A. W.; Mata, R. A.; May, A. J.; McNicholas, S. J.; Meyer, W.; Mura, M. E.; Nicklass,A.; Palmieri, P.; Pflüger, K.; Pitzer, R.; Reiher, M.; Schumann, U.; Stoll, H.; Stone, A. J.; Tarroni, R.; Thorsteinsson, T.; Wang, M.; Wolf, A. MOLPRO, a package of ab initio programs.

(25) Kresse, G.; Furthmuller, J. *Phys. Rev. B* **1996**, *54*, 11169.

(26) Lee, S. J.; Chung, H. Y.; Kim, K. S. *Bull. Korean Chem. Soc.* **2004**, *25*, 1061.

(27) Diefenbach, M.; Kim, K. S. *J. Phys. Chem. B* **2006**, *110*, 21639.

(28) (a) Kim, K. S.; Tarakeshwar, P.; Lee, J. Y. *Chem. Rev.* **2000**, *100*, 4145. (b) Lee, H. M.; Suh, S. B.; Lee, J. Y.; Tarakeshwar, P.; Kim, K. S. *J. Chem. Phys.* **2000**, *112*, 9759.

(29) (a) Mendizabal, F.; Pyykkö, P. *Phys. Chem. Chem. Phys.* **2004**, *6*, 900. (b) Hess, B. A.; Kaldor, U. *J. Chem. Phys.* **2000**, *112*, 1809.

(30) Luo, W.; Pennycook, S. J.; Pantelides, S. T. *Nano Lett.* **2007**, *7*, 3134.

(31) Kim, W. Y.; Kim, K. S. *Nat. Nanotechnol.* **2008**, *3*, 408.

CT8003113